Compensation for Magnetic Disturbances in Motion Estimation to Provide Feedback to Wearable Robotic Systems

Sebastjan Šlajpah, Roman Kamnik, *Member, IEEE*, and Marko Munih, *Member, IEEE*

***Abstract*— The direction of the Earth's magnetic field is used as a reference vector to determine the heading in orientation estimation with wearable sensors. However, the magnetic field strength is weak and can be easily disturbed in the vicinity of ferromagnetic materials, which may result in inaccurate estimate of orientation. This paper presents a novel method for estimating and compensating for magnetic disturbances. The compensation algorithm is implemented within a kinematic-based extended Kalman filter and is based on an assessment of the magnetic disturbance and the change of orientation in each time step. The proposed algorithm was experimentally validated by measuring the orientation of a simple mechanical system with three degrees of freedom in an artificially disturbed magnetic field. The results of the experimental evaluation show that an Kalman filter algorithm that incorporates compensating for magnetic disturbances is capable of estimating the orientation with moderate error (the absolute median errors $\Delta\tilde{\theta}_X$, $\Delta\tilde{\theta}_Z < 2°$, $\Delta\tilde{\theta}_Y < 9°$) when the Earth's magnetic field is disturbed by magnetic disturbance with a magnitude equal to twice the magnitude of the Earth's own magnetic field in different directions.**

***Index Terms*— Magnetic disturbance, inertial measurement unit, extended Kalman filter, orientation, sensory fusion.**

I. Introduction

THE development of microelectromechanical system (MEMS) components over the last decade has enabled the production of small and inexpensive low power sensors. MEMS sensors provide a low-cost, wearable, and easy-to-use alternative to expensive laboratory measurement systems. The technology enables their usage in various wearable systems, either worn by a user [1], [2] or integrated into robotic devices [3]–[6]. Wearable sensor systems for assessing human motion provide information about kinematic [7], [8] and kinetic parameters [9], e.g., joint angles and feet reactions.

Manuscript received February 19, 2015; revised March 22, 2016, September 22, 2016, and July 12, 2017; accepted October 2, 2017. Date of publication October 6, 2017; date of current version November 29, 2017. This work was supported in part by the Slovenian Research Agency (ARRS) under Grant 1000–11–310147, in part by the Research Programme Motion Analysis and Synthesis in Man and Machine under Grant P2–0228, and in part by the EU FP7 Project CYBERLEGs under Grant FP7–ICT–2011–7–287894. *(Corresponding author: Roman Kamnik.)*

The authors are with the Laboratory of Robotics, Department of Measurement and Robotics, Faculty of Electrical Engineering, University of Ljubljana, 1000 Ljubljana, Slovenia (e-mail: roman.kamnik@fe.uni-lj.si).

Digital Object Identifier 10.1109/TNSRE.2017.2760356

A typical wearable sensor is a combination of inertial and magnetic measurement units (IMUs) [7], [10]. IMU sensors output signals that are proportional to the angular velocity, translational acceleration, and magnetic field in 3D space. The raw signals are processed by using sensor fusion to determine the orientation of the sensor and the corresponding segment on which the sensor is mounted [7], [11]–[13].

The basic principle behind estimating 3D orientation [7], [11], [12], [14] uses the orientation estimated by integrating the measured angular velocity which is corrected using the orientation obtained from the measured acceleration and the measured magnetic field. To determine 3D orientation, two reference vectors are needed. The vector of gravitational acceleration to assess the inclination and the vector of the Earth's magnetic field to estimate the heading are commonly used.

Two major ussues emerge when using two reference vectors to estimate orientation: a) due to its principle of operation, the IMU accelerometer measures the sum of the gravitational and dynamic acceleration, and b) the Earth's weak magnetic field can be easily disturbed in the vicinity of ferromagnetic materials and electromagnetic devices, which are commonly used. The issue regarding the accelerometer is not problematic as long as the movement is quasi-static, so gravity is the dominant component of the measured acceleration [7], [14], [15]. Some authors separate movements into slow motion, where orientation is estimated from accelerometer measurements, and fast dynamic motion, where the orientation is assessed only by integration of the angular velocity [11], [16], [17]. This approach yields good results as long as dynamic movements do not last a long time and the integration drift does not induce error. Luinge [18] implemented a complementary Kalman filter design based on the modelling of errors. The errors were described by the difference of the estimates of inclination that were determined separately by the gyroscope and the accelerometer, and by the difference of the estimates of the magnetic vector that were determined separately by the gyroscope and the magnetometer. The results showed improvement in the estimated orientation.

In a previous study, we proposed an algorithm for determing kinematic parameters by using an extended Kalman filter that incorporates a kinematic model [12]. The method differentiates between gravitational and dynamic accelerations by estimating the latter from known kinematic relations of the observed

mechanism. The results showed that there was no drift over time of the kinematic parameters during dynamic and long-term movements.

Performing measurements in a controlled laboratory environment with little or no ferromagnetic materials in the vicinity minimizes the magnetic disturbances and thus improves the reliability of algorithms for estimating orientation [19]. However, in everyday life, sources of magnetic disturbances such as metal furniture, computers, electrical appliances, elevators, iron used in building construction, and cars are common [20], [21]. To prevent heading drift caused by the disturbed magnetic field when estimating orientation, several different methods were introduced.

Madgwick *et al.* [11] proposed using a gradient descent method in which the Earth's magnetic field was normalized such that the magnetic field vector has only two components. This was accomplished by summing the horizontal components. With this implementation, magnetic disturbances influence only the estimated heading of the orientation. The responsiveness of the algorithm is not optimal as the estimate ignores rapid changes in the magnetic field.

Instead of relying on the Earth's magnetic field vector, Schepers *et al.* [22] introduced a wearable magnetic system composed of three orthogonal coils that the user donned on their back. The relative orientation was updated by triggering magnetic pulses sequentially in the individual coils. The results showed a low root-mean-squared error in the estimated orientation (less than 5°); however, the additional magnetic module adds weight and increased the power consumption of the wearable system.

In [23], Yadav and Bleakley presented a particle filter-based correction method. A magnetic disturbance was detected by considering the magnetic dip angle and the magnetic field strength, and correction was performed using an adaptive cost function based on the variance determined during particle resampling.

Schiefer *et al.* [24] used a factored quaternion algorithm to obtain a heading estimate from the measured acceleration and magnetic field. The estimate was fused with the orientation calculated from integrating the gyroscope data using spherical linear interpolation. In the case of a magnetic disturbance, the influence of magnetometer is determined by setting suitable weighting factors. Additionally, the authors combined the use of zero-points (points with predefined known orientation) and a bidirectional computation to further improve the offline estimation accuracy.

Roetenberg *et al.* [25] used a complementary Kalman filter where magnetic disturbances were modeled as an autoregressive process based on the magnetic field strength and magnetic dip angle. The magnetic disturbance was modelled as a proportional combination of the magnetic disturbance determined in the previous calculation and white noise with an adaptive standard deviation. The proportion of the forwarded disturbance is characterized by moving the sensor module at different speeds and distances from ferromagnetic materials placed in the environment prior to measurement. When the disturbed magnetic field is detected, the standard deviation is increased relative to the change in the total magnetic flux and the magnetic dip angle. The algorithm performs well under different test conditions, but may not be accurate for dynamic motion, as the model of the magnetic disturbance is determined prior to usage for only a specific speed of motion and distance from the ferromagnetic material. Roetenberg *et al.* [26] further tested the performance of the algorithm in an environment simulating an assembly line. By implementing a magnetic disturbance model, the RMS error near a large metal object was less than 4°.

A non-uniform magnetic field that has been disturbed by magnetic interference prevents the accurate and reliable estimation of orientation and kinematic parameters. For this study, the kinematics-based Kalman filter presented in [12] was upgraded with a novel magnetic disturbance compensation method to enable the usage of IMUs in the vicinity of ferromagnetic materials and in a magnetically disturbed environment. The compensation algorithm and its implementation in the form of extended Kalman filter are described in the following sections. The performance of the proposed algorithm is experimentally evaluated by comparisons to the reference optical measurement system, the uncompensated approach, and an established gradient descent method.

II. Methods

A. Model of Magnetic Disturbance

Before performing measurements with IMUs, a global coordinate system $\mathrm{CS_G}$ is defined such that the vertical **y**-axis of the $\mathrm{CS_G}$ corresponds to the direction of gravity **g**; **z**-axis is aligned with the direction normal to the gravity vector **g** and the vector defined by the direction of the Earth's magnetic field **B**; and the **x**-axis is defined normal to the **y**- and **z**-axes. In this way, an orthogonal coordinate system is defined using axes aligned with gravity and the Earth's magnetic field. When initialized, the IMU is in a stationary position in an arbitrary orientation. The initial orientation $\mathbf{q}_0$ of the IMU with respect to the $\mathrm{CS_G}$ is determined from the measured acceleration and magnetic field vector $\mathbf{B}_{I,0}$ both expressed in the IMU's coordinate system $\mathrm{CS_I}$. Using this definitions, the Earth's magnetic field in the initial position can be expressed with respect to the $\mathrm{CS_G}$ by the quaternion transformation $\mathbf{B}_{G,0}$

$$\left[0, \mathbf{B}_{G,0}^{\mathrm{T}}\right]^{\mathrm{T}} = \mathbf{q}_0 \otimes \left[0, \mathbf{B}_{I,0}^{\mathrm{T}}\right]^{\mathrm{T}} \otimes \mathbf{q}_0^{*} \tag{1}$$

where $\otimes$ represents quaternion multiplication and $*$ denotes the quaternion conjugate. Quaternion notation is used to represent orientation to avoid singularities, which are common in other representations such as Euler angles or homogeneous matrices.

$\mathbf{B}_{G,0}$ is used to estimate the orientation at the subsequent time steps. In ideal conditions, the magnitudde and direction of the magnetic field vector are constant, which meanins that in any given time step $k-1$ $\mathbf{B}_{G,0} = \mathbf{B}_{G,k-1}$. In this case, the rotation $\mathbf{q}_{k-1}$ relates the measured $\mathbf{B}_{I,k-1}$ and the global $\mathbf{B}_{G,k-1}$

$$\left[0, \mathbf{B}_{I,k-1}^{\mathrm{T}}\right]^{\mathrm{T}} = \mathbf{q}_{k-1}^{*} \otimes \left[0, \mathbf{B}_{G,k-1}^{\mathrm{T}}\right]^{\mathrm{T}} \otimes \mathbf{q}_{k-1}. \tag{2}$$

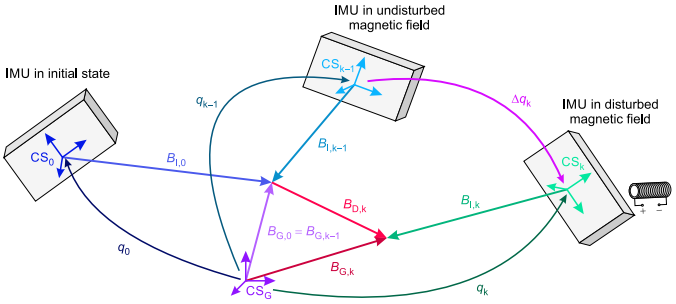

Fig. 1. An illustration of the measured magnetic field $\mathbf{B}_I$, the IMU's orientation $\mathbf{q}$, and the corresponding magnetic field transformed into the global coordinate system $\mathbf{B}_G$ at three different time steps: at the initial state ($k = 0$), at time $k-1$ without a magnetic disturbances, and at time k when the magnetic disturbance $\mathbf{B}_D$ is present.

When a magnetic disturbance $\mathbf{B}_{D,k}$ is introduced at time step k, the quaternion $\mathbf{q}_k$ no longer describes the relationship between the measured magnetic field $\mathbf{B}_{I,k}$ and Earth's magnetic field $\mathbf{B}_{G,0}$. As shown in Fig.1, the magnetic vector $\mathbf{B}_{G,k}$, which corresponds to the measured value $\mathbf{B}_{I,k}$ via (2), is the sum of the Earth's magnetic field $\mathbf{B}_{G,0}$ and magnetic disturbance $\mathbf{B}_{D,k}$, both expressed in $\mathrm{CS_G}$

$$\mathbf{B}_{G,k} = \mathbf{B}_{G,0} + \mathbf{B}_{D,k}. \tag{3}$$

Further, we model the magnetic disturbance $\mathbf{B}_{D,k}$ as

$$\mathbf{B}_{D,k} = \mathbf{B}_{D,k-1} + \dot{\mathbf{B}}_{D,k}\Delta t, \tag{4}$$

where $\mathbf{B}_{D,k-1}$ represents the magnetic disturbance at the previous time step $k-1$ and Δt is the length of a time step. The product $\dot{\mathbf{B}}_{D,k}\Delta t$ describes the change of the magnetic disturbance between the instants of time $k-1$ and k (see Fig.1) and is defined as

$$\dot{\mathbf{B}}_{D,k}\Delta t = \mathbf{B}_{G,k} - \mathbf{B}_{G,k-1}. \tag{5}$$

From the measured magnetic field $\mathbf{B}_{I,k-1}$ and the known orientation $\mathbf{q}_{k-1}$ at the previous time step $k-1$, the magnetic field $\mathbf{B}_{G,k-1}$ expressed in the $\mathrm{CS_G}$ is determined as

$$\left[0, \mathbf{B}_{G,k-1}^{\mathrm{T}}\right]^{\mathrm{T}} = \mathbf{q}_{k-1} \otimes \left[0, \mathbf{B}_{I,k-1}^{\mathrm{T}}\right]^{\mathrm{T}} \otimes \mathbf{q}_{k-1}^{*}. \tag{6}$$

Similarly, the magnetic vector corresponding to the measured values at instant k is determined as

$$\left[0, \mathbf{B}_{G,k}^{\mathrm{T}}\right]^{\mathrm{T}} = \hat{\mathbf{q}}_k \otimes \left[0, \mathbf{B}_{I,k}^{\mathrm{T}}\right]^{\mathrm{T}} \otimes \hat{\mathbf{q}}_k^{*}, \tag{7}$$

where $\hat{\mathbf{q}}_k$ represents the estimate of the current orientation. The orientation estimate can be modeled as the sum of the previous orientation $\mathbf{q}_{k-1}$ and the change in orientation between two time steps $\Delta\mathbf{q}_k$ (see Fig.1):

$$\hat{\mathbf{q}}_k = \mathbf{q}_{k-1} \otimes \Delta\mathbf{q}_k. \tag{8}$$

The estimate of the current orientation $\hat{\mathbf{q}}_k$ can be determined by numerical integration

$$\hat{\mathbf{q}}_k = \mathbf{q}_{k-1} + \dot{\mathbf{q}}_{k-1}\Delta t. \tag{9}$$

The quaternion $\dot{\mathbf{q}}_{k-1}$ represents the quaternion's time derivative

$$\dot{\mathbf{q}}_{k-1} = \frac{1}{2}\mathbf{q}_{k-1} \otimes \left[0, \boldsymbol{\omega}_{k-1}^{\mathrm{T}}\right]^{\mathrm{T}}, \tag{10}$$

where $\boldsymbol{\omega}_{k-1}$ represents measured angular velocity. By substituting (6), (7), and (9) into (5), the change in the magnetic disturbance can be written as (11), which is used in (4) to estimate the magnetic disturbance

$$\begin{aligned}\left[0, \dot{\mathbf{B}}_{D,k}^{\mathrm{T}}\right]^{\mathrm{T}}\Delta t &= \left(\mathbf{q}_{k-1} + \mathbf{q}_{k-1} \otimes \left[0, \boldsymbol{\omega}_k^{\mathrm{T}}\right]^{\mathrm{T}} \frac{\Delta t}{2}\right) \\ &\otimes \left[0, \mathbf{B}_{I,k}^{\mathrm{T}}\right]^{\mathrm{T}} \otimes \left(\mathbf{q}_{k-1} + \mathbf{q}_{k-1} \otimes \left[0, \boldsymbol{\omega}_k^{\mathrm{T}}\right]^{\mathrm{T}} \frac{\Delta t}{2}\right)^{*} \\ &- \mathbf{q}_{k-1} \otimes \left[0, \mathbf{B}_{I,k-1}^{\mathrm{T}}\right]^{\mathrm{T}} \otimes \mathbf{q}_{k-1}^{*}. \end{aligned} \tag{11}$$

The relationship between the measured magnetic field and the Earth's magnetic field (2) is thus extended into a form that compensates for magnetic disturbances

$$\left[0, \mathbf{B}_{I,k}^{\mathrm{T}}\right]^{\mathrm{T}} = \mathbf{q}_k^{*} \otimes \left[0, \mathbf{B}_{G,0}^{\mathrm{T}} + \mathbf{B}_{D,k}^{\mathrm{T}}\right]^{\mathrm{T}} \otimes \mathbf{q}_k. \tag{12}$$

B. Extended Kalman Filter Implementation

An extended Kalman filter algorithm (EKF) [27] is used to estimate orientation by constantly fusing data from the gyroscope, accelerometer, and magnetometer. The EKF comprises three parts: a) integration of the angular velocity, which is a classical approach for determining orientation by using Kalman filtering, b) fusion of the measured acceleration based on known kinematic relations [12], and c) fusion of the measured magnetic field based on a magnetic disturbance model (12). The estimation model incorporates a non-linear state-space represemntation of the state and measurement equations

$$\begin{aligned}\mathbf{x}_k &= \mathbf{f}\left(\mathbf{x}_{k-1}, \mathbf{u}_{k-1}, \mathbf{w}_{k-1}\right) \\ \mathbf{z}_k &= \mathbf{h}\left(\mathbf{x}_k, \mathbf{v}_k\right). \end{aligned} \tag{13}$$

The non-linear function $\mathbf{f}$ describes the relationship among the current state $\mathbf{x}_k$, the previous state $\mathbf{x}_{k-1}$, the input vector $\mathbf{u}_{k-1}$, and superimposed process noise $\mathbf{w}_{k-1}$. The function $\mathbf{h_k}$ relates the state $\mathbf{x}_k$ to the measurements $\mathbf{z}_k$ at time step k, with addition of superimposed measurement noise $\mathbf{v}_k$.

The state vector $\mathbf{x}_k$, which incorporates angular dynamics and a description of orientation, is extended by the magnetic disturbance $\mathbf{B}_D$ and the time derivative of the magnetic disturbance $\dot{\mathbf{B}}_D$

$$\mathbf{x}_k = \left[\boldsymbol{\omega}_k^{\mathrm{T}}\, \dot{\boldsymbol{\omega}}_k^{\mathrm{T}}\, \mathbf{q}_k^{\mathrm{T}}\, \dot{\mathbf{q}}_k^{\mathrm{T}}\, \ddot{\mathbf{q}}_k^{\mathrm{T}}\, \mathbf{B}_{D,k}^{\mathrm{T}}\, \dot{\mathbf{B}}_{D,k}^{\mathrm{T}}\right]^{\mathrm{T}}. \tag{14}$$

In (14), the $\dot{\boldsymbol{\omega}}_k$ represents the time derivative of the angular velocity $\boldsymbol{\omega}_k$, and $\dot{\mathbf{q}}_k$ and $\ddot{\mathbf{q}}_k$ are the first and second time derivative of quaternion $\mathbf{q}_k$. The function $\mathbf{f}$ is expanded by including (4) and (11), as shown in (15), as shown at the bottom of the next page. The indices in square brackets indicate the components of the vector function $\mathbf{f}$.

The measurement vector $\mathbf{z}_k$ includes all of the measured quantities: the angular velocity $\boldsymbol{\omega}_{I,k}$ and it's time derivative $\dot{\boldsymbol{\omega}}_{I,k}$, acceleration $\mathbf{a}_{I,k}$, and magnetic field vector $\mathbf{B}_{I,k}$

$$\mathbf{z}_k = \left[\boldsymbol{\omega}_{I,k}^{\mathrm{T}} \dot{\boldsymbol{\omega}}_{I,k}^{\mathrm{T}} \mathbf{a}_{I,k}^{\mathrm{T}} \mathbf{B}_{I,k}^{\mathrm{T}}\right]^{\mathrm{T}}. \tag{16}$$

The relationship among measurements $\mathbf{z}_k$ and states $\mathbf{x}_k$ are described by function $\mathbf{h}_k$ in (17). The components $\mathbf{h}_{[7-9]}$ relate the acceleration, as measured by IMU $\mathbf{a}_{I,k}$, which is a combination of the gravitational and dynamic acceleration with calculated values based on the known motion kinematics of a mechanism segment (linear acceleration of the joint $\mathbf{a}_{J,k}$, angular velocity $\boldsymbol{\omega}_k$, and angular acceleration $\dot{\boldsymbol{\omega}}_k$) and known position vector $\mathbf{r}$ from joint to the IMU describing the placement of the IMU on the segment. The components $\mathbf{h}_{[10-12]}$ relate the measured values of the magnetic field vector $\mathbf{B}_{I,k}$ and the outputs of the disturbed magnetic field model (12).

$$\begin{bmatrix} \mathbf{h}_{[1-3]} \\ \mathbf{h}_{[4-6]} \\ \mathbf{h}_{[7-9]} \\ \left[0, \mathbf{h}^{\mathrm{T}}_{[10-12]}\right]^{\mathrm{T}} \end{bmatrix} = \begin{bmatrix} \boldsymbol{\omega}_k \\ \dot{\boldsymbol{\omega}}_k \\ \mathbf{a}_{J,k} + \boldsymbol{\omega}_k \times (\boldsymbol{\omega}_k \times \mathbf{r}) + \dot{\boldsymbol{\omega}}_k \times \mathbf{r} - \mathbf{g}_k \\ \mathbf{q}^*_k \otimes \left[0, \mathbf{B}^{\mathrm{T}}_{G,0} + c_{E,k}\mathbf{B}^{\mathrm{T}}_{D,k}\right]^{\mathrm{T}} \otimes \mathbf{q}_k \end{bmatrix} \tag{17}$$

In addition to (12), the parameter $c_{E,k}$ is introduced in relation $\mathbf{h}_{[10-12]}$ to enable or disable the compensation of magnetic disturbances. The value of $c_{E,k} \in \{0, 1\}$ is determined depending on the amplitude of the magnetic field $|\mathbf{B}_{I,k}|$ as

$$c_{E,k} \begin{cases} 0, & \text{for } |\mathbf{B}_{I,k}| \in \left[|\mathbf{B}_{G,0}| \pm 0.1|\mathbf{B}_{G,0}|\right] \\ 1, & \text{otherwise.} \end{cases} \tag{18}$$

The algorithm for magnetic disturbance compensation is thus enabled ($c_{E,k} = 1$) when the measured amplitude of the magnetic field $|\mathbf{B}_{I,k}|$ deviates by more than 10% from the amplitude of the initial magnetic field $|\mathbf{B}_{G,0}|$, determined at the beginning of the algorithm's run time.

The novel EKF with magnetic compensation has two additional states, i.e., $\mathbf{f}_{[19-21]}$ and $\mathbf{f}_{[22-24]}$, when compared to the EKF without compensation. The components $\mathbf{h}_{[10-12]}$ introduce the magnetic disturbance as part of a measured magnetic vector, which can be omitted for the non-compensated EKF by setting the $c_{E,k} = 0$.

The schematic presentation of the Kalman filter is depicted in Fig.2. The set of equations for discrete-time implementation was presented in our previous work [12].

C. Experimental Validation

Experiments were performed to test the performance of proposed orientation estimation with magnetic disturbance compensation. For validation, a mechanical pendulum was built using extruded aluminium as a non-ferromagnetic material and a 3D printed gimbal joint with additional longitudinal rotation. The pendulum segment was mounted onto the fixed aluminium frame, which allowed the three rotational degrees of freedom of motion (DOF).

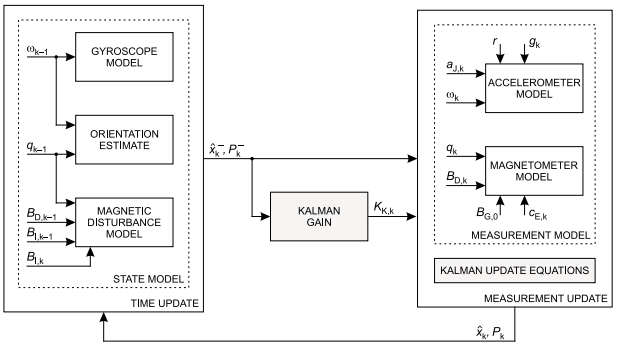

Fig. 2. Structure of the EKF with included magnetic compensation. The state model is described by equation (15) which includes: the gyroscope model $\mathbf{f}_{[1-6]}$, the orientation estimate $\mathbf{f}_{[7\text{-}18]}$, and the magnetic disturbance model $\mathbf{f}_{[19-24]}$. Models of the accelerometer with included kinematic relationships and the magnetic model are described in (17) by $\mathbf{h}_{[4-6]}$ and $\mathbf{f}_{[7-9]}$, respectively. Vectors $\hat{\mathbf{x}}_k^-$ and $\mathbf{P}_k^-$ denote *a priori*, $\hat{\mathbf{x}}_k$ and $\mathbf{P}_k$ denote *a posteriori* state and error covariance vectors. Equations for the kalman gain $K_{K,k}$ and the kalman update are presented in previous work [12].

The IMU was mounted on the pendulum at a displacement of distance $\mathbf{r} = 30$ cm from the joint centre as shown in Fig.3. The IMU incorporated a three-axis gyroscope (measurement range $\pm 500\ ^\circ\mathrm{s}^{-1}$), three-axis accelerometer (measurement range ± 4 G; G $\approx 9.81\ \mathrm{m/s}^2$), and a three-axis magnetometer (measurement range ± 0.13 mT) [14]. The size of the IMU was ($30 \times 20 \times 5$) mm and its weight was 6 g. Data were wirelessly transferred to a data acquisition unit with a 100 Hz refresh rate.

As a reference, an optical measuring system Optotrak Certus (Northern Digital Inc., Waterloo, Canada) was used. Three active infrared markers were placed on a plastic plate and securely mounted on the pendulum (see Fig.3). The reference orientation of the pendulum was calculated on-line baed on the acquired positions of the markers. The sampling frequency of the reference measuring system was 100 Hz, and the RMS precision of acquired markers' positions was below 0.1 mm.

A solenoidal coil was used (diameter 32 cm, height 5 cm, coil constant $k_{DC} = 1.2$ mT/A) to introduce magnetic

$$\begin{bmatrix} \mathbf{f}_{[1-3]} \\ \mathbf{f}_{[4-6]} \\ \mathbf{f}_{[7-10]} \\ \mathbf{f}_{[11-14]} \\ \mathbf{f}_{[15-18]} \\ \mathbf{f}_{[19-21]} \\ \mathbf{f}_{[22-24]} \end{bmatrix} = \begin{bmatrix} \boldsymbol{\omega}_{k-1} + \dot{\boldsymbol{\omega}}_{k-1}\Delta t \\ \dot{\boldsymbol{\omega}}_{k-1} \\ \mathbf{q}_{k-1} + \dot{\mathbf{q}}_{k-1}\Delta t \\ \frac{1}{2}\mathbf{q}_{k-1} \otimes \left[0,\ \boldsymbol{\omega}_{k-1}\right]^{\mathrm{T}} \\ \frac{1}{2}\dot{\mathbf{q}}_{k-1} \otimes \left[0,\ \boldsymbol{\omega}_{k-1}\right]^{\mathrm{T}} + \frac{1}{2}\mathbf{q}_k \otimes \left[0,\ \dot{\boldsymbol{\omega}}_k\right]^{\mathrm{T}} \\ \mathbf{B}_{D,k-1} + \dot{\mathbf{B}}_{D,k-1}\Delta t \\ \left(\left(\mathbf{q}_{k-1} + \mathbf{q}_{k-1} \otimes \left[0, \boldsymbol{\omega}^{\mathrm{T}}_{k-1}\right]^{\mathrm{T}} \frac{1}{2}\Delta t\right) \otimes \left[0, \mathbf{B}^{\mathrm{T}}_{I,k}\right]^{\mathrm{T}} \right. \\ \left. \otimes \left(\mathbf{q}_{k-1} + \mathbf{q}_{k-1} \otimes \left[0, \boldsymbol{\omega}^{\mathrm{T}}_{k-1}\right]^{\mathrm{T}} \frac{1}{2}\Delta t\right)^* - \mathbf{q}_{k-1} \otimes \left[0, \mathbf{B}^{\mathrm{T}}_{I,k-1}\right]^{\mathrm{T}} \otimes \mathbf{q}^*_{k-1}\right) \Delta t^{-1} \end{bmatrix} \tag{15}$$

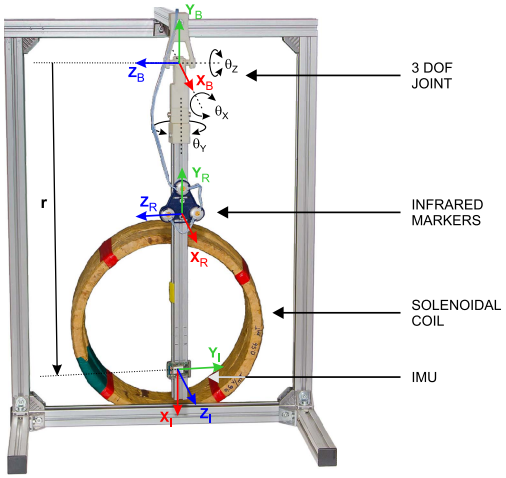

Fig. 3. Experimental setup incorporating a pendulum, an IMU, infrared markers, and a solenoidal coil for estimating orientation with superimposed magnetic disturbances. The individual coordinate systems of the IMU, reference markers, and base are denoted with subscripts *I*, *R*, and *B*, respectively. The orientation was represented using Euler angles (marked as θ_X, θ_Y, θ_Z). The placement of the IMU on the pendulum is denoted with **r**.

disturbances into the system. The coil was placed in different orientations within a radius of 40 cm from the equilibrium position of the pendulum and was set to have a magnetic field strength of $B_{coil} \approx 1.2$ mT at the centre. Due to the dissipation of the magnetic field, the amplitude of the measured magnetic field at the equilibrium position was on the order of twice Earth's magnetic field ($|\mathbf{B}_I| \approx 2|\mathbf{B}_{G,0}|$).

The experimental protocol included 4 sets of measurements of duration at least 180 s each. During each set of measurements, the pendulum was manually swung to rotate randomly about all three axes with the following limitations: around the **x**- and **z**-axes the rotations were limited to $\pm 40°$, and around **y**-axis, they were limited to $\pm 90°$. The limitations were determined by the limited viewing angle of the reference measuring system. Each set was composed of three 60 s long measurements of 24 ± 4 (mean $\pm$ standard deviation) dynamic swings around each individual axis separated by several seconds (6.5 s $\pm$ 1.6 s), where the pendulum remained still. The first set was a reference measurement, where orientation was obtained with no magnetic disturbance present. During the other three sets of measurements, an artificial magnetic disturbance was imposed in different directions such that the main magnetic axis of the coil was parallel to the global **x**-, **y**-, and **z**-axes, as illustrated in the upper part of Fig.4. An additional set of measurements was performed where magnetic disturbances were imposed by a large metal box with dimensions $(49 \times 40 \times 35)$ cm positioned at a distance of 3 cm from pendulum along the **x**-axis. The pendulum was manually swung in the frontal and transverse plane which can be considered equivalent to abduction/adduction and flexion/extension of the human arm in the study by Roetenberg *et al.* [26]. The aforementioned movement was composed of 20 repetitions of each movement. During each session, the orientation was assessed and computed in four different ways: i) via active markers as a reference, ii) via kinematic-based EKF, presented in [12], i.e., without compensation of magnetic disturbances, iii) using the upgraded EKF with included active compensation of the magnetic disturbances, and iv) using the algorithm based on the gradient method presented in [11]. The gradient method was tuned based on reference measurements; the optimal gain value was set to $\beta = 0.81$.

In the data analysis, the estimated pendulum orientations were compared with the reference measurements. For statistical validation, the absolute errors with respect to the reference are calculated for each sample and test condition. The output orientations were denoted by quaternions, but for easier interpretation, the results were converted into Euler angles. For case iii), only the values obtained when the magnetic disturbance was detected ($c_{E,k} = 1$) are used in the statistical analysis. The absolute errors between the reference and estimated angles in each instant of time are presented with box plots. Orientations determined using the gradient descent method were also included for comparison. To validate the performance under dynamic conditions, the similarity of the angle trajectories obtained using the with reference system and the proposed method was evaluated by using Pearson's correlation coefficient (PCC). PCC is utilized to describe the similarity of two signal profiles and comprises the values $PCC \in [-1, 1]$, where 1 represents an identical profile and -1 represents the opposite profile. All data processing was accomplished using the Matlab R2013a software (MathWorks, USA).

III. Results

The results for one 210 s long data set are shown as an example in Fig.4. For each dynamic swinging example four cases of magnetic conditions were investigated: in Earth's magnetic field without magnetic disturbances (case i) and with imposed magnetic disturbances in directions aligned with the global **x**-, **y**-, and **z**-axis (cases ii–iv). Before activating the coil to mimic magnetic disturbances in the different direction, the coil was manually moved into an initial position. The upper three graphs compare the orientation angle trajectories of the pendulum obtained using the reference system (marked as OPTOTRAK), the extended Kalman filter with no magnetic compensation (marked as EKF-NC), and the extended Kalman filter with integrated compensation (marked as EKF-C). Thus, subplots a), b), and c) illustrate rotations around the **x**-, **y**-, and **z**-axes of the global coordinate system, i.e., angles θ_X, θ_Y, and θ_Z, respectively. The length of the measured magnetic field vector $|\mathbf{B}_I|$ normalized to the length of the Earth's magnetic field vector $|\mathbf{B}_{G,0}|$ is shown in subplot d).

In Fig.5, the absolute errors for the compensated ($\Delta\theta_{\mathrm{C}}$) and non-compensated ($\Delta\theta_{\mathrm{NC}}$) approaches, and the gradient descent method ($\Delta\theta_{\mathrm{GRAD}}$) are presented for different testing conditions (without magnetic disturbances, magnetic disturbances imposed by the coil in different directions, and with the metal box are shown for each assessed rotation ($\Delta\theta_X$, $\Delta\theta_Y$, $\Delta\theta_Z$).

In Table I, the absolute median errors $\Delta\tilde{\theta}$ and root-mean-square (RMS) errors $\Delta\theta_{\mathrm{RMS}}$ for each angle for the aforementioned conditions are collected. Table I also shows Pearson's correlation coefficient PCC describing similarities in the joint angle trajectories for all test conditions.

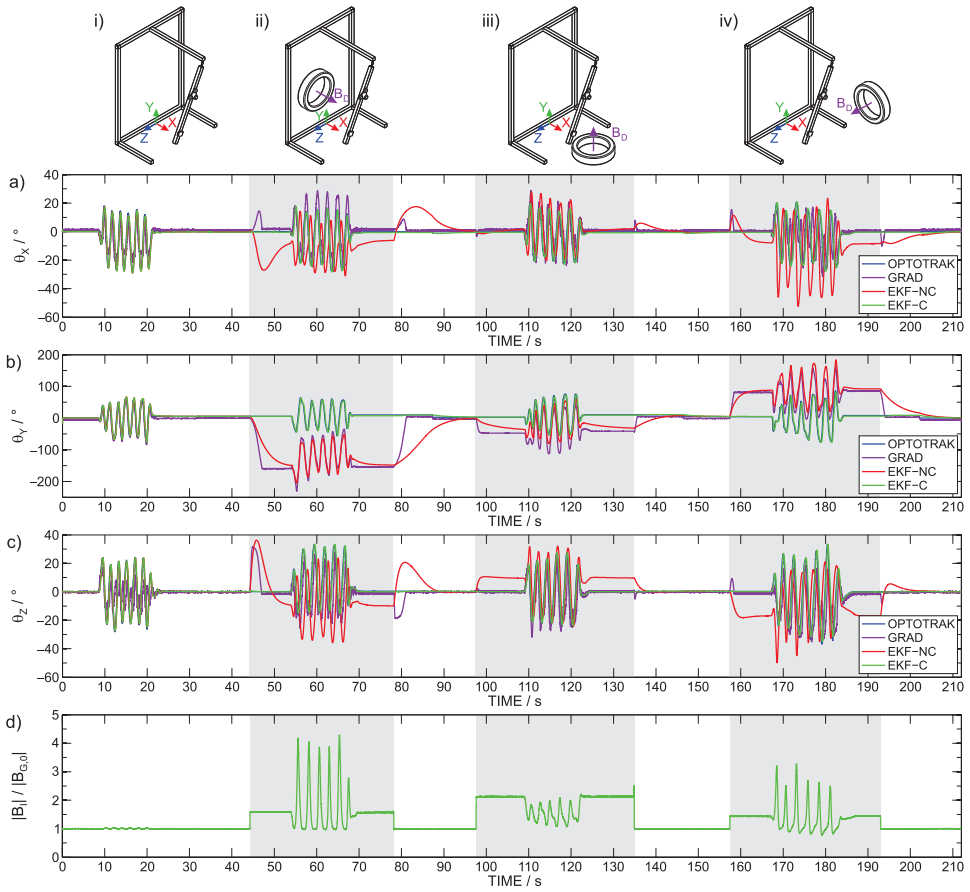

Fig. 4. Angles of the pendulum around the **x**-, **y**-, and **z**-axes (subplots a), (b), and (c), respectively) obtained using the reference system (OPTOTRAK), gradient descent method (GRAD), EKF with no magnetic disturbances compensation (EKF-NC), and EKF using the magnetic disturbances compensation algorithm (EKF-C) under four different conditions: i) no magnetic disturbance (0 s to 44 s), ii) a magnetic disturbance along **x**-axis (44 s to 78 s), iii) a magnetic disturbance along **y**-axis (97 s to 135 s), and iv) a magnetic disturbance along **z**-axis (157 s to 193 s). Subplot d) shows the change in the amplitude of the measured magnetic field during the experiment. The grey areas mark the time intervals of active compensation of the magnetic disturbances ($c_{E,k} = 1$). Data presented in this figure are for illustration purposes only, to show angle drift during magnetic disturbance, and do not show the actual measurements used in the data analysis.

IV. Discussion

Earth's magnetic field can easily be disturbed in the vicinity of ferromagnetic materials which are present at home or in the public environment. For example, experimental measurements of the amplitude of the magnetic field in a parking lot full of cars show that the amplitude can deviate from $|\mathbf{B}_I| \in [0.8, 1.4]\,|\mathbf{B}_{G,0}|$ and that in an elevator, the amplitude can deviate from $|\mathbf{B}_I| \in [0.03, 1.1]\,|\mathbf{B}_{G,0}|$. Homogeneity of the magnetic field is of great importance because most orientation estimation algorithms use the direction of the magnetic field as a reference for heading information. In this paper, a method for magnetic disturbance compensation was implemented based on the detected change of the amplitude of the measured magnetic field, the known previous orientation, and the estimated change of orientation. The model of the magnetic disturbance covers any change to the global magnetic field regardless of the source. The model includes any spatial or temporal variations of the Earth's magnetic field, external magnetic sources, or changes due to vicinity of ferromagnetic materials. It thus provides a versatile solution for orientation measurements under non-homogeneous conditions. The proposed method was implemented into extended Kalman filter with incorporated kinematic model. The performance of a compensated and non-compensated version of the algorithm was compared under different test conditions.

Roetenberg *et al.* [25] introduced a method for compensating for magnetic disturbances by weighting the influence of the magnetometer. In the case of detected magnetic disturbances, less weight was assigned to the magnetometer output, and the orientation estimate relied primarily on the gyroscope and accelerometer data. The algorithm presented in this work does not alter the influence of the individual sensor's data on the estimated orientation. The magnitude of a magnetic disturbance is constantly assessed based on sensor measurements, and the results are further used to correct the global magnetic field corresponding to the measured magnetic field as described with (12). The compensated magnetic reference thus provides a more accurate orientation estimate during movements.

Magnetic disturbances were generated using magnetic coil. The mean amplitude of the measured magnetic field throughout all measurements was $|\mathbf{B}_I| = 1.43|\mathbf{B}_G|$ with a standard of deviation $0.50|\mathbf{B}_G|$. The minimum and maximum values were $0.62|\mathbf{B}_G|$ and $11.76|\mathbf{B}_G|$, respectively. For experiments using

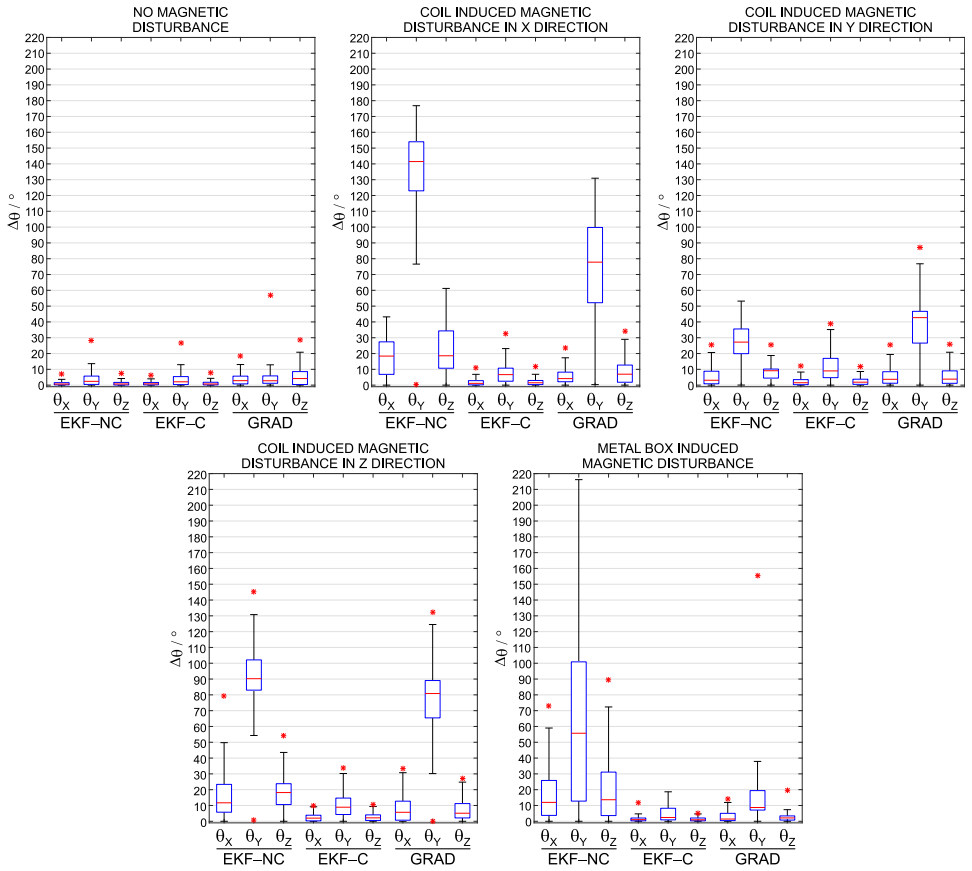

Fig. 5. Absolute angle errors $\Delta\theta$ between the reference measurements and angles calculated using EKF without (EKF-NC) and with (EKF-C) compensation for the magnetic disturbances and the gradient descent method [11] (GRAD) for five different conditions, as illustrated using boxplots. The middle line, the bottom and the top of the box present the median, 25th and 75th percentile, respectively. The whiskers represent the furthermost value in the 1.5 interquartile ranges. The red asterisk denotes outliers representing the minimum or maximum values.

TABLE I

ABSOLUTE MEDIAN ERROR $\Delta\tilde{\theta}$, RMS ERROR $\Delta\theta_{\mathrm{RMS}}$, AND PEARSON'S CORRELATION COEFFICIENT *PCC* FOR ANGLE ESTIMATION BETWEEN REFERENCE ANGLES AND ANGLES OBTAINED WITH THE EKF WITHOUT AND WITH COMPENSATION OF THE MAGNETIC DISTURBANCES AND GRADIENT DESCENT METHOD [11] FOR FIVE CONDITIONS: WITHOUT MAGNETIC DISTURBANCES $\mathbf{B}_D$, WITH MAGNETIC DISTURBANCES ALONG **x**-, **y**-, AND **z**-AXES, MARKED WITH $\mathbf{B}_{D,X}$, $\mathbf{B}_{D,Y}$, AND $\mathbf{B}_{D,Z}$, RESPECTIVELY, AND WITH PRESENCE OF THE METAL BOX

		EKF WITHOUT COMPENSATION			EKF WITH COMPENSATION			GRADIENT METHOD		
		$\Delta\tilde{\theta}/^\circ$	$\Delta\theta_{\mathrm{RMS}}/^\circ$	PCC	$\Delta\tilde{\theta}/^\circ$	$\Delta\theta_{\mathrm{RMS}}/^\circ$	PCC	$\Delta\tilde{\theta}/^\circ$	$\Delta\theta_{\mathrm{RMS}}/^\circ$	PCC
No $\mathbf{B}_D$	θ_X	1.61	2.45	0.98	1.55	2.49	0.98	3.92	6.92	0.80
	θ_Y	4.84	8.40	0.97	4.39	8.27	0.97	3.84	8.25	0.96
	θ_Z	1.68	2.65	0.98	1.58	2.57	0.98	5.88	10.80	0.76
$\mathbf{B}_{D,X}$	θ_X	16.29	20.34	−0.72	0.93	2.51	0.98	3.67	6.73	0.89
	θ_Y	138.41	134.36	0.66	5.78	8.75	0.96	72.88	78.23	0.75
	θ_Z	17.22	26.37	−0.56	1.29	2.73	0.97	6.13	10.18	0.63
$\mathbf{B}_{D,Y}$	θ_X	2.67	6.95	0.84	1.14	2.91	0.97	2.92	7.08	0.77
	θ_Y	25.50	27.56	0.92	8.25	11.33	0.94	39.30	40.04	0.78
	θ_Z	8.07	9.34	0.78	1.40	2.99	0.96	2.92	7.23	0.68
$\mathbf{B}_{D,Z}$	θ_X	10.06	21.46	−0.20	1.60	2.98	0.97	4.55	10.07	0.48
	θ_Y	87.59	89.22	0.79	8.53	11.27	0.98	80.30	77.72	0.72
	θ_Z	17.68	20.84	0.30	1.77	3.14	0.97	4.19	8.80	0.76
Metal box	θ_X	12.07	23.04	0.85	1.65	3.14	0.97	1.43	4.46	0.58
	θ_Y	56.09	78.46	−0.47	2.41	6.77	0.93	8.76	22.11	−0.57
	θ_Z	13.75	25.83	0.23	0.96	1.70	0.99	2.14	4.17	0.62

a metal box placed in the vicinity, the amplitude of magnetic field was $|\mathbf{B}_I| = (1.62 \pm 0.81)|\mathbf{B}_G|$; $|\mathbf{B}_I| \in [0.40, 4.61]\,|\mathbf{B}_G|$. To determine whether the experimental magnetic field was representative, we compared it with measured data acquired in real world situations. The magnetic field measured on the left foot of a healthy subject while walking on a polygon which

incorporated level walking, negotiating stairs, and turning (as presented in study [12]) was $|\mathbf{B}_I| = (1.05 \pm 0.15)|\mathbf{B}_G|$, $|\mathbf{B}_I| \in [0.07, 2.82]\,|\mathbf{B}_G|$. The magnetic field measured in study [28] at the feet of a person following transtibial amputation who walked using of prosthesis between parallel bars was $|\mathbf{B}_I| = (0.96 \pm 0.38)|\mathbf{B}_G|$, $|\mathbf{B}_I| \in [0.09, 1.91]\,|\mathbf{B}_G|$ on the sound side of the person, whereasthe measured values were higher on the side with the prosthesis $|\mathbf{B}_I| = (3.19 \pm 0.44)|\mathbf{B}_G|$, $|\mathbf{B}_I| \in [1.74, 4.18]\,|\mathbf{B}_G|$. Comparison of the values shows that the magnetic field generated with a magnetic coil is comparable to the magnetic field measured in real world situations.

The example shown in Fig.4 demonstrates that magnetic disturbances can cause large errors in orientation estimation (up to 180°), especially around the vertical axis. The disturbed magnetic field mostly influences the heading estimation, whereas other two directions are less affected. The magnitude of the influence depends on the direction of the disturbance: as the magnetic field determines the orientation around the vertical axis, the disturbances acting in the horizontal plane cause greater errors than the one acting in the vertical direction. The example shows that magnetic disturbances have a large impact on estimating orientation before movement, when the pendulum was in a static state, and during dynamic motion, when the pendulum was swinging.

The results of the statistical anaylsis in Fig.5 and Table I show that both EKFs (with and without compensation) are comparable and perform well with small errors (absolute median error below 2° for angles around the horizontal axes and approximately 5° around the vertical axis) when no magnetic disturbance is present. When the magnetic coil was positioned in the way that the imposed magnetic field was aligned with a particular horizontal axis (**x**- or **z**-axis, case ii or iv), substantial errors with large dispersion were observed in the estimated angles around the vertical axis for the non-compensated EKF (absolute median error $\Delta\tilde{\theta}_Y = 138.4°$ with $\mathbf{B}_{D,X}$ and $\Delta\tilde{\theta}_Y = 87.6°$ with $\mathbf{B}_{D,Z}$). Angles around horizontal axes were estimated more accurately but still with substantial errors and dispersion ($\Delta\tilde{\theta}_X$, $\Delta\tilde{\theta}_Z \approx 18°$). Similar trends with larger dispersions were also be observed when the pendulum was swinging in the vicinity of the metal box. In the cases where the magnetic field was disturbed along the vertical axis, the estimated orientation was influenced less and yielded smaller errors ($\Delta\tilde{\theta}_Y = 25.5°$) since the imposed magnetic field affected only the measured inclination of the Earth's magnetic field vector. The large values of the errors indicate that the EKF without compensation is not suitable for orientation estimation when operating in the disturbed Earth's magnetic field.

In contrast, the results show that the EKF which incorporates compensation of magnetic disturbances performed well even in disturbed magnetic fields. The absolute median errors of rotation angles assessment around the **x**- and **z**-axes are below 2° ($\Delta\theta_{\mathrm{RMS}} < 3°$) with small dispersion regardless of the direction of the magnetic disturbance. The median of the angle errors for the estimates of rotations around the vertical axis are higher ($\Delta\tilde{\theta}_Y < 9°$ for coil, $\Delta\tilde{\theta}_Y < 2.5°$ for metal box) but still significantly smaller compared to the orientation errors for the EKF without compensation ($\Delta\tilde{\theta}_Y \in [25,\ 139]\,°$).

Orientation was also estimated using the gradient descent method. This method was used for comparison since it yields similar performance to the EKF or particle filter based methods discussed in [23], but it provides a less computationally demanding solution, which makes it more convenient for wearable applications. The comparison with reference angles shows that the gradient descent method performs better than the EKF without compensation in disturbed magnetic fields. Statistical analysis (Fig.5 and Table I) shows that the proposed method is superior to the gradient descent method in terms of accuracy and robustness in a disturbed magnetic field.

The PCC results prove that the angle trajectories obtained with the EKF with magnetic compensation match the reference angle trajectories for each individual axis regardless of the direction or source of the disturbance. For the **x**- and **z**-axes the similarity was determined to be $PCC_{X,Z} \approx 0.97$, whereas for the **y**-axis $PCC_Y > 0.93$. In contrast, the statistical results show that the EKF without compensation has inferior performance when magnetic disturbances are present. In some cases the PCC of the EKF without compensation is negative which indicates the high impact of magnetic disturbances on orientation estimation.

The convergence of the proposed algorithm was assessed based on the number of samples required for the absolute error between the estimated angle θ and angle in steady state $\bar{\theta}$ to be below 5% of $\bar{\theta}$: $||\theta - \bar{\theta}|| \leq 0.05\,\bar{\theta}$. The analysis showed good convergence times: convergence was achieved on average within 348 samples (maximum 915 samples) after the introduction of a magnetic disturbance.

V. Conclusions

Wearable systems comprising small MEMS sensors are gaining popularity for monitoring human activities in their environment outside the laboratory. Magnetic disturbances induced by nearby ferromagnetic materials present a large problem when estimating orientation using IMUs since sensor fusion algorithms use the Earth's magnetic field as a reference vector for heading information. This paper introduces a novel approach to compensate for magnetic disturbances by integrating the compensationinto an extended Kalman filter. The algorithm is based on an estimate of the magnetic disturbance and the change of orientation. Experimental results show that an EKF with incorporated compensation of magnetic disturbances is capable of orientation assessment with moderate error ($\Delta\tilde{\theta}_X$, $\Delta\tilde{\theta}_Z < 2°$, $\Delta\tilde{\theta}_Y < 9°$) when the applied disturbance in different direction is twice that of the Earth's magnetic field. Compared with the non-compensated EKF, the latter results in larger errors ($\Delta\tilde{\theta}_X \in [3, 17]\,°$, $\Delta\tilde{\theta}_Y \in [25, 139]\,°$, $\Delta\tilde{\theta}_Z \in [8, 18]\,°$). The added relations in the proposed approach increases the computational complexity of orientation estimation algorithm. The number of required multiplications and summations is nearly doubled from 51026 and 47200 in the uncompensated version to 102308 and 91941 for the version with magnetic compensation. However, the required number of operations is still within the computational capabilities of present day microcontroller platforms operating with a sampling rate of up to 100 Hz, which is an acceptable

refresh rate for feedback systems. The results show that the method has stable performance and is robust against magnetic disturbances compared to the EKF without compensation. The proposed algorithm for orientation estimation with magnetic disturbance compensation can thus be used in combination with wearable sensors to acquire human motion kinematic parameters or to provide feedback for the control of wearable robots, regardless of the surrounding environment. In addition, the proposed approach can be applied in other areas where the orientation assessment with wearable sensors is not possible due to extraneous magnetic fields.

References

[1] P. Bonato, "Wearable sensors and systems," *IEEE Eng. Med. Biol. Mag.*, vol. 29, no. 3, pp. 25–36, May 2010.

[2] S. Patel, H. Park, P. Bonato, L. Chan, and M. Rodgers, "A review of wearable sensors and systems with application in rehabilitation," *J. Neuroeng. Rehabil.*, vol. 9, no. 1, p. 21, 2012.

[3] E. C. Martinez-Villalpando and H. Herr, "Agonist-antagonist active knee prosthesis: A preliminary study in level-ground walking," *J. Rehabil. Res. Develop.*, vol. 46, no. 3, pp. 361–373, 2009.

[4] J. C. Moreno, E. R. de Lima, A. F. Ruíz, F. J. Brunetti, and J. L. Pons, "Design and implementation of an inertial measurement unit for control of artificial limbs: Application on leg orthoses," *Sensor. Actuat. B, Chem.*, vol. 118, nos. 1–2, pp. 333–337, 2006.

[5] H. Kazerooni and R. Steger, "The Berkeley lower extremity exoskeleton," *J. Dyn. Syst., Meas., Control*, vol. 128, no. 1, pp. 14–25, 2006.

[6] M. Goršič *et al.*, "Online phase detection using wearable sensors for walking with a robotic prosthesis," *Sensors*, vol. 14, no. 2, pp. 2776–2794, 2014.

[7] H. J. Luinge and P. H. Veltink, "Measuring orientation of human body segments using miniature gyroscopes and accelerometers," *Med. Biol. Eng. Comput.*, vol. 43, no. 2, pp. 273–282, Mar. 2005.

[8] T. Seel, J. Raisch, and T. Schauer, "IMU-based joint angle measurement for gait analysis," *Sensors*, vol. 14, no. 4, pp. 6891–6909, Jan. 2014.

[9] S. Crea *et al.*, "Development of an experimental set-up for providing lower-limb amputees with an augmenting feedback," in *Converging Clinical and Engineering Research on Neurorehabilitation*. Berlin, Germany: Springer, 2013, pp. 321–325.

[10] T. Beravs, J. Podobnik, and M. Munih, "Three-axial accelerometer calibration using Kalman filter covariance matrix for online estimation of optimal sensor orientation," *IEEE Trans. Instrum. Meas.*, vol. 61, no. 9, pp. 2501–2511, Sep. 2012.

[11] S. O. Madgwick, A. J. Harrison, and R. Vaidyanathan, "Estimation of IMU and MARG orientation using a gradient descent algorithm," in *Proc. IEEE Int. Conf. Rehabil. Robot. (ICORR)*, Jun. 2011, pp. 1–7.

[12] S. Šlajpah, R. Kamnik, and M. Munih, "Kinematics based sensory fusion for wearable motion assessment in human walking," *Comput. Methods Programs Biomed.*, vol. 116, no. 2, pp. 131–144, 2014.

[13] J. Cockcroft, J. H. Müller, and C. Scheffer, "A novel complimentary filter for tracking hip angles during cycling using wireless inertial sensors and dynamic acceleration estimation," *IEEE Sensors J.*, vol. 14, no. 8, pp. 2864–2871, Aug. 2014.

[14] T. Beravs, P. Reberšek, D. Novak, J. Podobnik, and M. Munih, "Development and validation of a wearable inertial measurement system for use with lower limb exoskeletons," in *Proc. 11th IEEE-RAS Int. Conf. Humanoid Robots (Humanoids)*, Oct. 2011, pp. 212–217.

[15] D. Roetenberg, P. J. Slycke, and P. H. Veltink, "Ambulatory position and orientation tracking fusing magnetic and inertial sensing," *IEEE Trans. Biomed. Eng.*, vol. 54, no. 5, pp. 883–890, May 2007.

[16] E. R. Bachmann, "Inertial and magnetic tracking of limb segment orientation for inserting humans into synthetic environments," Ph.D. dissertation, Naval Postgraduate school, Monterey, CA, USA, 2000.

[17] K. J. O'Donovan, R. Kamnik, D. T. O'Keeffe, and G. M. Lyons, "An inertial and magnetic sensor based technique for joint angle measurement," *J. Biomech.*, vol. 40, no. 12, pp. 2604–2611, 2007.

[18] H. J. Luinge, "Inertial sensing of human movement," Ph.D. dissertation, Faculty Elect. Eng., Math. Comput. Sci., Univ. Twente, Enschede, The Nederlands, 2002.

[19] R. Zhu and Z. Zhou, "A real-time articulated human motion tracking using tri-axis inertial/magnetic sensors package," *IEEE Trans. Neural Syst. Rehabil. Eng.*, vol. 12, no. 2, pp. 295–302, Jun. 2004.

[20] W. H. K. de Vries, H. E. J. Veeger, C. T. M. Baten, and F. C. T. van der Helm, "Magnetic distortion in motion labs, implications for validating inertial magnetic sensors," *Gait Posture*, vol. 29, no. 4, pp. 535–541, 2009.

[21] E. R. Bachmann, X. Yun, and C. W. Peterson, "An investigation of the effects of magnetic variations on inertial/magnetic orientation sensors," in *Proc. IEEE Int. Conf. Robot. Autom. (ICRA)*, vol. 2. Apr./May 2004, pp. 1115–1122.

[22] H. M. Schepers, D. Roetenberg, and P. H. Veltink, "Ambulatory human motion tracking by fusion of inertial and magnetic sensing with adaptive actuation," *Med. Biol. Eng. Comput.*, vol. 48, no. 1, pp. 27–37, 2010.

[23] N. Yadav and C. Bleakley, "Accurate orientation estimation using ahrs under conditions of magnetic distortion," *Sensors*, vol. 14, no. 11, pp. 20008–20024, 2014.

[24] C. Schiefer *et al.*, "Optimization of inertial sensor-based motion capturing for magnetically distorted field applications," *J. Biomech. Eng.*, vol. 136, no. 12, p. 121008, 2014.

[25] D. Roetenberg, H. J. Luinge, C. T. M. Baten, and P. H. Veltink, "Compensation of magnetic disturbances improves inertial and magnetic sensing of human body segment orientation," *IEEE Trans. Neural Syst. Rehabil. Eng.*, vol. 13, no. 3, pp. 395–405, Sep. 2005.

[26] D. Roetenberg, C. T. M. Baten, and P. H. Veltink, "Estimating body segment orientation by applying inertial and magnetic sensing near ferromagnetic materials," *IEEE Trans. Neural Syst. Rehabil. Eng.*, vol. 15, no. 3, pp. 469–471, Sep. 2007.

[27] G. Welch and G. Bishop, "An introduction to the Kalman filter," Dept. Comput. Sci., Univ. North Carolina at Chapel Hill, Chapel Hill, NC, USA, 2006.

[28] L. Ambrožič *et al.*, "CYBERLEGs: A user-oriented robotic transfemoral prosthesis with whole-body awareness control," *IEEE Robot. Autom. Mag.*, vol. 21, no. 4, pp. 82–93, Dec. 2014.

Sebastjan Šlajpah received the B.Sc. and Ph.D. degrees from the University of Ljubljana, Ljubljana, Slovenia, in 2011 and 2015, respectively. He is currently a Teaching Assistant with the Laboratory of Robotics, Department of Measurement and Robotics, Faculty of Electrical Engineering, University of Ljubljana. His research interests include robotics, sensory fusion, and movement analysis.

Roman Kamnik received the D.Sc. degree in electrical engineering from the University of Ljubljana, Slovenia, in 1999. He is currently a Full Professor with the Laboratory of Robotics, Faculty of Electrical Engineering, University of Ljubljana. His research interests include biomedical engineering and robotics.

Marko Munih received the Ph.D. degree in electrical engineering from the University of Ljubljana (UL), Ljubljana, Slovenia. He is currently a Full Professor and the Head of the Laboratory of Robotics, UL.

His industrial expertise includes applications of robots in construction and robots for measurement tasks. Recently, his attention was directed to the use of inertial measurement units for movement assessment. His research is oriented into robot contact with environment, as well as the design and use of haptic interfaces in the fields of industry and rehabilitation engineering.